Research Square

Preprints are preliminary reports that have not undergone peer review.
They should not be considered conclusive, used to inform clinical practice,
or referenced by the media as validated information.

Comparative Analysis of Generalized Thermoelasticity Models for Heat Conduction in a Circular Micro-Plate Using Kirchhoff–Love Plate Theory

Hamdy Youssef

hmyoussef@uqu.edu.sa

Umm al-Qura University

Research Article

Keywords: Thermoelasticity, Silicon, Microplate resonator, Kirchhoff's Love plate, Ramp-type heat, Refined Green-Lindsay, Biot, Lord-Sulman, Green-Naghdi T, Moore–Gibson–Thompson

Posted Date: November 5th, 2026

DOI: https://doi.org/10.21203/rs.3.rs-11139784/v1

License: This work is licensed under a Creative Commons Attribution 4.0 International License.
Read Full License

Additional Declarations: No competing interests reported.

Comparative Analysis of Generalized Thermoelasticity Models for Heat Conduction in a Circular Micro-Plate Using Kirchhoff–Love Plate Theory

Abstract

This research introduces a comprehensive mathematical model for examining heat conduction and thermomechanical properties in an isotropic, homogeneous, thermoelastic circular microplate, grounded on the Kirchhoff–Love plate theory. The formulation integrates many generalized thermoelasticity models, such as Green–Lindsay, Biot, Lord–Shulman, Green–Naghdi Type-I, Green–Naghdi Type-III, and Moore–Gibson–Thompson theories, into a coherent framework of governing differential equations. The examination employs scaled thermoelasticity for a circular micro-plate that is supported at its periphery and exposed to ramp-type thermal loading. The Laplace transform method is used to provide analytical solutions for the governing equations, while Tzou's iterative approach is employed for the numerical inversion of the Laplace transform to assess the transient thermoelastic response. A comprehensive parametric analysis examines the influence of ramp-time heating, plate thickness, and material characteristics on thermomechanical wave transmission in a silicon microplate. We provide visual comparisons of several thermoelastic models to emphasize their dynamic properties and commonalities in mechanical behavior. The findings reveal that the Green–Naghdi Type-III and Moore–Gibson–Thompson models have the most similar mechanical behavior, followed by the Biot and Lord–Shulman models. Moreover, the research indicates that ramp-time heating and geometric factors may proficiently modulate thermomechanical wave transmission in micro-scale architectures.

Keywords: Thermoelasticity; Silicon; Microplate resonator; Kirchhoff's Love plate; Ramp-type heat; Refined Green-Lindsay; Biot, Lord-Sulman; Green-Naghdi T; Moore–Gibson–Thompson.

Introduction

Circular microplates are used in many forms of electromechanical microresonators. Hao performed an investigation on thermoelastic damping in relation to vibrations inside circular thin-plate resonators used in micro- and nano-electromechanical systems [1]. Sun and Tohmyoh conducted a survey of thermoelastic damping in circular-plate resonators, focusing specifically on axisymmetric vibration [2]. Sun and Saka examined the impact of thermoelastic damping on vertical oscillation using circular plate resonators[3]. The thermoelastic damping of vibrations in a circular thin plate with generalized viscothermoelastic properties was calculated by Grover [4-6]. Guo et al. formulated a thermoelastic theory of damping for micro- and nano-resonators using a dual-phase-lag model. Subsequently, they examined the circular dissipation of the microplate resonator [7,8]. Biot is credited with introducing the integrated theory of thermoelasticity. This theory combines the equations of elasticity and heat conduction, which have been validated by physical tests. It demonstrates that changes in temperature cause strain in an elastic body, and conversely, strain in an elastic body causes temperature changes. The notion of linked thermoelasticity is beneficial for several issues [9]. The equations of this theory include a hyperbolic partial differential equation representing the equation of motion, and a parabolic equation representing the equation of energy conservation. The inherent properties of the heat equation suggest that if an infinitely extended elastic material is subjected to a thermal or mechanical disturbance, the effect would propagate immediately to infinity, contradicting experimental findings. This demonstrates the need for a novel hyperbolic energy equation [9]. Many recent applications have been solved within this theorem [10-14]. Lord and Shulman introduced the notion of generalized thermoelasticity for an isotropic material by including a singular relaxation interval [15]. Dhaliwal and Sherief extended this theory to include the anisotropic case [16]. Cattaneo's theory of heat conduction supersedes Fourier's heat conduction equation by including both the heat flux and its temporal derivative. The heat equation associated with this theory is hyperbolic, therefore addressing the dilemma of infinite propagation velocities in both scenarios [17]. Many recent applications have been solved in the context of Lord-Shulman thermoelasticity [14,18-27]. The second generalization in the linked elasticity theory is the thermoelasticity theory characterized by two relaxation periods, sometimes referred to as temperature-rate-dependent thermoelasticity. In an investigation into the thermodynamics of thermoelastic substances, Müller proposed an inequality for entropy generation. This inequality was used to establish constraints on a particular collection of constitutive equations [28]. Green and Laws proposed a generalization of this inequality [29].

Green and Lindsay obtained an explicit version of the constitutive equations [30]. These equations were obtained independently by Suhubi [31]. This hypothesis includes two constants that function as relaxation times and modify all equations inside the coupled theory, not only the heat equation. The traditional Fourier's law of thermal conduction holds true when the examined medium has a center of symmetry. Several contemporary utilizations of the Green-Lindsay theorem are enumerated in the references [14,18,19,25,32-39]. Green and Naghdi postulated a new concept in generalized thermoelasticity, called thermoelasticity without energy dissipation [40]. The primary feature of this theory is that, in contrast to conventional thermoelasticity grounded on Fourier's heat conduction equation, heat transfer does not lead to energy loss. Moreover, the stress tensor, obtained from the same potential function, is used to formulate the constitutive equation for the entropy flow vector. Furthermore, the theory permits the transmission of heat as thermal waves at constrained speeds. The comprehensive discourse centers on nonlinear theory, followed by the exposition of linear theory. Green and Naghdi introduce the idea via the use of the global entropy balance [40,41]. Despite the extensive basic progress, the practical application is confined to heat transfer in a stationary, rigid solid via conduction and the transmission of heat pulses as thermal waves at a finite speed. Three unique types of constitutive response functions are suggested. Type-I, subsequent to the linearization of the theory, aligns with the traditional heat conduction theory, which is based on Fourier's law. Conversely, types II and III permit the propagation of thermoelastic disturbances at a constrained speed. Both type-II and type-III theories of heat transfer in a stationary rigid solid permit a restricted wave speed; however, only the type-II theory excludes energy dissipation [14,40-44]. Youssef introduced a new theory of thermoelasticity based on the fractional order of strain (fraction-order Duhamel-Neumann stress-strain relation) [45].

The present study develops a unified mathematical framework for analyzing the thermoelastic vibration behaviour of a circular silicon microplate resonator within the context of seven different thermoelasticity theories. Unlike previous investigations that typically employ a single thermoelastic model or limited comparative approaches, the proposed formulation introduces a generalized governing equation capable of representing the coupled thermoelasticity theory of Biot, the Lord–Shulman model, the Green–Naghdi types I and III theories, the simple and refined Green–Lindsay theories, and the Moore–Gibson–Thompson theory within a single consistent structure. The model is established based on Kirchhoff–Love plate theory and applied to a supported circular microplate subjected to ramp-type thermal

loading. Furthermore, the study provides a systematic comparative analysis of the thermo-mechanical responses predicted by these seven theories under identical physical and geometric conditions, enabling the identification of key parameters—such as ramp-time heating, plate thickness, and spatial location—that significantly influence the propagation of thermal and mechanical waves in micro-scale resonator systems. This unified formulation provides a comprehensive framework for evaluating the relative behaviour of multiple thermoelastic models and supports the design and optimization of micro- and nano-scale thermoelastic devices. Part of this work has been pre-reviewed in (https://www.researchsquare.com/article/rs-6787626/private/timeline)

Generalized thermoelastic based on seven theorems.

We consider an isotropic, homogeneous, and thermoelastic circular microplate, supported under the Kirchhoff-Love plate. The centre of the plate is at the origin with uniform thickness $z\left(-\frac{h}{2}\le z\le\frac{h}{2}\right)$ and radius $r\left(0\le r\le a\right)$, and in the system of cylindrical coordinates $\left(r,\ \theta,\ z\right)$(see Figure 1).

Thus, all the studied functions are in the following domain [46-48]:

$$\Psi=\left\{\left(r,\theta,z\right):0\le r\le a,\ \ 0\le\theta\le 2\pi,\ -\frac{h}{2}\le z\le\frac{h}{2}\right\}. \tag{1}$$

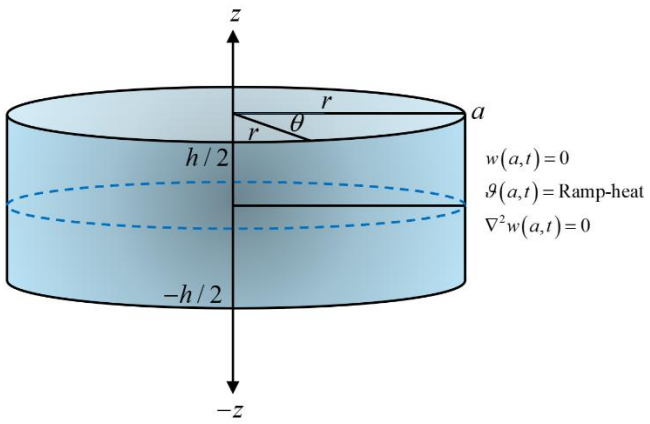


Figure 1: The isotropic, homogeneous, and thermoelastic supported circular micro-plate

Assuming the plate is in a state of no tension and no strain, and is at an equilibrium temperature T_0. The smooth, unaffected surface is kept on the plane $\left(r,\theta\right)$, and the *z*-axis is considered normal to that surface, as in Figure 1 [29][46,49].

Therefore, the displacement components are as follows [4]:

$$\left(u_r, u_\theta, u_z\right) = \left(-z\frac{\partial w}{\partial r}, -\frac{z}{r}\frac{\partial w}{\partial \theta}, w\right), \tag{2}$$

where $w = w\left(r, \theta, z, t\right)$ is the lateral deflection function (vibration) in the general case.

The temperature increment $\varphi\left(r, \theta, z, t\right)$ concerning the absolute temperature T and the reference temperature T_0 is in the form:

$$\varphi = \left(T - T_0\right) \text{ such that } \left|T - T_0\right| \ll T_0 \ . \tag{3}$$

The stress components are [4, 29-33]:

$$\sigma_{rr} = \frac{E}{1-\upsilon}\left[\frac{\varepsilon_{rr} + \upsilon\varepsilon_{\theta\theta}}{1+\upsilon} - \alpha_T\varphi\right], \tag{4}$$

$$\sigma_{\theta\theta} = \frac{E}{1-\upsilon}\left[\frac{\varepsilon_{\theta\theta} + \upsilon\varepsilon_{rr}}{1+\upsilon} - \alpha_T\varphi\right], \tag{5}$$

and

$$\sigma_{r\theta} = \frac{E\varepsilon_{r\theta}}{1+\upsilon}, \qquad \sigma_{zz} = \sigma_{rz} = \sigma_{z\theta} = 0\,. \tag{6}$$

The strain components are:

$$\left(\varepsilon_{rr}, \varepsilon_{\theta\theta}, \varepsilon_{zz}\right) = \left(\frac{\partial u_r}{\partial r}, \frac{u_r}{r} + \frac{1}{r}\frac{\partial u_\theta}{\partial \theta}, \frac{\partial^2 u_z}{\partial z^2}\right) = \left(-z\frac{\partial^2 w}{\partial r^2}, -z\left(\frac{1}{r^2}\frac{\partial^2 w}{\partial \theta^2} + \frac{1}{r}\frac{\partial w}{\partial r}\right), 0\right), \tag{7}$$

and

$$\left(\varepsilon_{r\theta}, \varepsilon_{rz}, \varepsilon_{z\theta}\right) = \left(\frac{1}{r}\frac{\partial u_r}{\partial \theta} + \frac{\partial u_\theta}{\partial r} - \frac{u_\theta}{r}, 0, 0\right) = \left(-2z\frac{\partial}{\partial r}\left(\frac{1}{r}\frac{\partial w}{\partial \theta}\right), 0, 0\right), \tag{8}$$

while the volumetric dilatation is given by:

$$\varepsilon = \varepsilon_{rr} + \varepsilon_{\theta\theta} + \varepsilon_{zz}\,. \tag{9}$$

The equation of motion is [29, 30, 34, 35]:

$$\left(\frac{\partial^2}{\partial r^2} + \frac{2}{r}\frac{\partial}{\partial r}\right)M_r + \frac{2}{r}\left(\frac{1}{r}\frac{\partial}{\partial \theta} + \frac{\partial^2}{\partial \theta\,\partial r}\right)M_{r\theta} + \frac{1}{r}\left(\frac{1}{r}\frac{\partial^2}{\partial \theta^2} - \frac{\partial}{\partial r}\right)M_\theta - \rho h\ddot{w} = 0\,, \tag{10}$$

where the following formulas give the moments of flexure and torsion [1-4,6,7,50,51]:

$$M_r = \int_{-h/2}^{h/2} z\ \sigma_{rr}\, dz = -\frac{h^3 E}{12\left(1-\upsilon^2\right)}\left[\left(\frac{\partial^2}{\partial r^2} + \frac{\upsilon}{r}\left(\frac{\partial}{\partial r} + \frac{1}{r}\frac{\partial^2}{\partial \theta^2}\right)\right)w + \left(1+\upsilon\right)\alpha_T M_T\right], \tag{11}$$

$$M_{r\theta} = \int_{-h/2}^{h/2} z\,\sigma_{r\theta}\, dz = -\frac{h^3 E}{12\left(1+\upsilon\right)}\left[\frac{\partial}{\partial r}\left(\frac{1}{r}\frac{\partial w}{\partial r}\right)\right], \tag{12}$$

and

$$M_\theta = \int_{-h/2}^{h/2} z\,\sigma_{\theta\theta}\,dz = -\frac{h^3 E}{12\left(1-\upsilon^2\right)}\left[\left(\upsilon\frac{\partial^2}{\partial r^2}+\frac{1}{r}\frac{\partial}{\partial r}+\frac{1}{r^2}\frac{\partial^2}{\partial\theta^2}\right)w+\left(1+\upsilon\right)\alpha_T M_T\right], \quad (13)$$

where α_T gives the coefficient of thermal expansion, υ is Poisson's ratio, ρ shows the density, and E expresses the well-known Young's modulus.

Moreover, M_T gives the thermal moment and is defined by the following formula [1-4,6,7,50,51]:

$$M_T = \frac{12}{h^3}\int_{-h/2}^{h/2} z\,\varphi\,dz\,. \quad (14)$$

By inserting equations (11)-(13) into the equation (10) and considering the refined temperature function, we get the equation of motion in the following form [36-39]:

$$E\nabla^2\left(\nabla^2 w\right)+\frac{12\alpha_T\left(1+\upsilon\right)}{h^3}E\nabla^2\left(\left(\varepsilon_1+\sum_{n=1}^{N}\frac{\tau_1^n}{n!}\frac{\partial^n}{\partial t^n}\right)\int_{-h/2}^{h/2}\varphi\,z\,dz\right)+\frac{12\rho\left(1-\upsilon^2\right)}{h^2}\ddot{w}=0\,. \quad (15)$$

Therefore, the differential equation of the motion (15) has the following form:

$$\nabla^2\left(\nabla^2 w\right)+\frac{12\alpha_T\left(1+\upsilon\right)}{h^3}\nabla^2\left(\left(\varepsilon_1+\sum_{n=1}^{N}\frac{\tau_1^n}{n!}\frac{\partial^n}{\partial t^n}\right)\int_{-h/2}^{h/2}\varphi\,z\,dz\right)+\frac{12\rho\left(1-\upsilon^2\right)}{h^2 E}\ddot{w}=0\,, \quad (16)$$

and the stress components are in the forms [36-39]:

$$\sigma_{rr} = \frac{E_0}{1-\upsilon}\left[\frac{\varepsilon_{rr}+\upsilon\varepsilon_{\theta\theta}}{1+\upsilon}-\alpha_T\left(\varepsilon_1+\sum_{n=1}^{N}\frac{\tau_1^n}{n!}\frac{\partial^n}{\partial t^n}\right)\varphi\right], \quad (17)$$

and

$$\sigma_{\theta\theta} = \frac{E_0}{1-\upsilon}\left[\frac{\upsilon\varepsilon_{rr}+\varepsilon_{\theta\theta}}{1+\upsilon}-\alpha_T\left(\varepsilon_1+\sum_{n=1}^{N}\frac{\tau_1^n}{n!}\frac{\partial^n}{\partial t^n}\right)\varphi\right], \quad (18)$$

and the heat conduction equation will be in the following form [36-39]:

$$\left(\frac{\partial}{\partial t}+\frac{K^*}{K}\right)\left(\nabla^2+\frac{\partial^2}{\partial z^2}\right)\varphi=\left(1+\tau_q\frac{\partial}{\partial t}\right)\left(\begin{array}{c}\frac{\rho C_E}{K}\left(\varepsilon_1+\sum_{n=1}^{N}\frac{\tau_1^n}{n!}\frac{\partial^n}{\partial t^n}\right)\ddot{\varphi}+\\ \frac{T_0\gamma}{K}\left(\varepsilon_2+\sum_{m=1}^{M}\frac{\tau_2^{m-1}}{(m-1)!}\frac{\partial^{m-1}}{\partial t^{m-1}}\right)\ddot{\varepsilon}\end{array}\right). \quad (19)$$

The unified equation (19) can be applied to the coupled thermoelasticity (CTE) of Biot, generalized thermoelasticity with one relaxation time of Lord-Shulman(L-S), Green-Naghdi

type-I (G-N-I), Green-Naghdi type-III (G-N-III), simple Green-Lindsy (S-G-L), refined Green-Lindsy (R-G-L), and Moore–Gibson–Thompson (M-G-T) [52-55], as follows:

(i) $K^{*}=0,\tau_q=\tau_1=\tau_2=0,\ \varepsilon_1=\varepsilon_2=1$, gives Biot's theorem (CTE) for heat conduction.

(ii) $K^{*}=0,\tau_q\neq 0,\ \tau_1=\tau_2=0,\ \varepsilon_1=\varepsilon_2=1$, gives the Lord-Shulman theorem (L-S) for heat conduction.

(iii) $K^{*}=0,\tau_q=0,\ \tau_1=1,\tau_2=1,\ \varepsilon_1=\varepsilon_2=0,N=1,M=2$, gives the Green-Naghdi (G-N-I) heat conduction [55,56].

(iv) $K^{*}\neq 0,\ \tau_q=\tau_1=\tau_2=0,\ \varepsilon_1=\varepsilon_2=1$, gives the Green-Naghdi (G-N-III) heat conduction [55,56].

(v) $K^{*}=0,\ \tau_q=0,\tau_1\neq 0,\ \tau_2\neq 0,\ \varepsilon_1=1,\ \varepsilon_2=0,\ N=M=1$, gives the simple Green-Lindsay (S-G-L) heat conduction [36-39].

(vi) $K^{*}=0,\tau_q=0,\tau_1\neq 0,\ \tau_2\neq 0,\ \varepsilon_1=1,\ \varepsilon_2=0,\ N>1,M=1$, gives the Refined Green-Lindsay (R-G-L) heat conduction [36-39].

(vii) $K^{*}\neq 0,\tau_q\neq 0,\ \tau_1=\tau_2=0,\ \varepsilon_1=\varepsilon_2=1$, gives the Moore–Gibson–Thompson (M-G-T) heat conduction [57].

We may take $K^{*}=\dfrac{C_E\left(\lambda+2\mu\right)}{4}$ as the main character of the Green-Naghdi theory, where K gives the thermal conductivity, C_E denotes the specific heat at constant deformation, and the parameter τ_q is known as the relaxation time of the thermal wave, while $\nabla^2=\dfrac{\partial^2}{\partial r^2}+\dfrac{1}{r}\dfrac{\partial}{\partial r}+\dfrac{1}{r^2}\dfrac{\partial^2}{\partial\theta^2}$.

Now, for the axisymmetric micro-circular plate, the components of the displacement are in the form [4]:

$$\left(u_r,u_\theta,u_z\right)=\left(-z\frac{\partial w\left(r,t\right)}{\partial r},0,w\left(r,t\right)\right), \tag{20}$$

while the components of the strain are in the following form:

$$\left(\varepsilon_{rr},\varepsilon_{\theta\theta},\varepsilon_{zz}\right)=\left(-z\frac{\partial^2 w}{\partial r^2},-\frac{z}{r}\frac{\partial w}{\partial r},0\right), \tag{21}$$

and

$$\left(\varepsilon_{r\theta},\varepsilon_{rz},\varepsilon_{z\theta}\right)=\left(0,0,0\right). \tag{22}$$

Hence, we obtain:

$$\varepsilon = \varepsilon_{rr} + \varepsilon_{\theta\theta} + \varepsilon_{zz} = -z\nabla^2 w, \tag{23}$$

where the operator ∇^2 has the following new form:

$$\nabla^2 = \frac{\partial^2}{\partial r^2} + \frac{1}{r}\frac{\partial}{\partial r}. \tag{24}$$

The heat flux through the two surfaces $z = \pm h/2$ of the circular plate does not exist, which gives:

$$\left.\frac{\partial \varphi(r,z,t)}{\partial z}\right|_{z=\pm h/2} = 0\ . \tag{25}$$

Where the circular plate thickness is too small compared to its radius, we can assume the temperature varies as a function of $\sin(pz)$ the thickness direction of the plate z [1, 2, 3, 4, 5], thus, we can consider that:

$$\varphi(r,z,t) = \vartheta(r,t)\sin(pz), \quad p = \pi/h\,. \tag{26}$$

Hence, the equation of motion (16) changes to the following new form:

$$\nabla^2\left(\nabla^2 w\right) + \frac{12(1+\upsilon)\alpha_T}{h^3}\left(\varepsilon_1 + \sum_{n=1}^{N}\frac{\tau_1^n}{n!}\frac{\partial^n}{\partial t^n}\right)\nabla^2\vartheta\left(\int_{-h/2}^{h/2} z\sin(pz)\,dz\right) + \frac{12\rho\left(1-\upsilon^2\right)}{h^2 E}\ddot{w} = 0\,. \tag{27}$$

After executing the integration in the middle term of the above equation, we obtain:

$$\nabla^2\left(\nabla^2 w\right) + \frac{24(1+\upsilon)\alpha_T}{\pi^2 h}\left(\varepsilon_1 + \sum_{n=1}^{N}\frac{\tau_1^n}{n!}\frac{\partial^n}{\partial t^n}\right)\nabla^2\vartheta + \frac{12\rho\left(1-\upsilon^2\right)}{h^2 E}\ddot{w} = 0\,. \tag{28}$$

The equation of heat conduction (19) could be in the following form:

$$\left(\frac{\partial}{\partial t} + \frac{K^*}{K}\right)\left(\nabla^2 + \frac{\partial^2}{\partial z^2}\right)\varphi = \left(1 + \tau_q\frac{\partial}{\partial t}\right)\left(\begin{array}{l}\dfrac{\rho C_E}{K}\left(\varepsilon_1 + \displaystyle\sum_{n=1}^{N}\frac{\tau_1^n}{n!}\frac{\partial^n}{\partial t^n}\right)\ddot{\varphi} \\ \qquad -\dfrac{zT_0\gamma}{K}\left(\varepsilon_2 + \displaystyle\sum_{m=1}^{M}\frac{\tau_2^{m-1}}{(m-1)!}\frac{\partial^{m-1}}{\partial t^{m-1}}\right)\nabla^2\ddot{w}\end{array}\right). \tag{29}$$

Then, we have:

$$\nabla^2\left(\nabla^2 w\right) + \frac{24(1+\upsilon)\alpha_T}{\pi^2 h}\nabla^2\left(\varepsilon_1 + \sum_{n=1}^{N}\frac{\tau_1^n}{n!}\frac{\partial^n}{\partial t^n}\right)\vartheta + \frac{12\rho\left(1-\upsilon^2\right)}{h^2 E}\ddot{w} = 0\,, \tag{30}$$

$$\left(\frac{\partial}{\partial t}+\frac{K^*}{K}\right)\left(\nabla^2-p^2\right)\varphi=\left(1+\tau_q\frac{\partial}{\partial t}\right)\left(\begin{array}{l}\dfrac{\rho C_E}{K}\left(\varepsilon_1+\displaystyle\sum_{n=1}^{N}\frac{\tau_1^n}{n!}\frac{\partial^n}{\partial t^n}\right)\ddot{\varphi}\\ \qquad -\dfrac{zT_0\gamma}{K\sin(pz)}\left(\varepsilon_2+\displaystyle\sum_{m=1}^{M}\frac{\tau_2^{m-1}}{(m-1)!}\frac{\partial^{m-1}}{\partial t^{m-1}}\right)\nabla^2\ddot{w}\end{array}\right), \tag{31}$$

$$\sigma_{rr}=\frac{E}{1-\upsilon^2}\left[-z\frac{\partial^2 w}{\partial r^2}-\frac{\upsilon z}{r}\frac{\partial w}{\partial r}-\alpha_T(1+\upsilon)\left(\varepsilon_1+\sum_{n=1}^{N}\frac{\tau_1^n}{n!}\frac{\partial^n}{\partial t^n}\right)\varphi\right], \tag{32}$$

and

$$\sigma_{\theta\theta}=\frac{E}{1-\upsilon^2}\left[-z\upsilon\frac{\partial^2 w}{\partial r^2}-\frac{z}{r}\frac{\partial w}{\partial r}-\alpha_T(1+\upsilon)\left(\varepsilon_1+\sum_{n=1}^{N}\frac{\tau_1^n}{n!}\frac{\partial^n}{\partial t^n}\right)\varphi\right]. \tag{33}$$

The following new dimensionless variables may be used as follows [44, 45]:

$$\sigma_{ij}=E\sigma'_{ij},\ \vartheta=T_o\vartheta',\ \left(t,\tau_q,\tau_1\right)\equiv\frac{1}{\eta c_o^2}\left(t',\tau'_q,\tau'_1\right),\left(r,z,w,h,a,\frac{1}{p}\right)\equiv\frac{1}{\eta c_o}\left(r',z',w',h',a',\frac{1}{p'}\right) \tag{34}$$

where $c_o^2=\dfrac{E}{\rho}$, $\eta=\dfrac{\rho C_E}{K}$.

which gives that:

$$\nabla^2\nabla^2 w+\alpha_1\left(\varepsilon_1+\sum_{n=1}^{N}\frac{\tau_1^n}{n!}\frac{\partial^n}{\partial t^n}\right)\nabla^2\vartheta+\alpha_2\ddot{w}=0, \tag{35}$$

$$\left(\frac{\partial}{\partial t}+\alpha_3\right)\left(\nabla^2-p^2\right)\vartheta=\left(1+\tau_q\frac{\partial}{\partial t}\right)\left[\left(\varepsilon_1+\sum_{n=1}^{N}\frac{\tau_1^n}{n!}\frac{\partial^n}{\partial t^n}\right)\ddot{\vartheta}-\alpha_4\left(\varepsilon_2+\sum_{m=1}^{M}\frac{\tau_2^{m-1}}{(m-1)!}\frac{\partial^{m-1}}{\partial t^{m-1}}\right)\nabla^2\ddot{w}\right], \tag{36}$$

$$\sigma_{rr}=\frac{1}{1-\upsilon^2}\left[-z\frac{\partial^2 w}{\partial r^2}-\frac{\upsilon z}{r}\frac{\partial w}{\partial r}-\alpha_5\left(\varepsilon_1+\sum_{n=1}^{N}\frac{\tau_1^n}{n!}\frac{\partial^n}{\partial t^n}\right)\varphi\right], \tag{37}$$

and

$$\sigma_{\theta\theta}=\frac{1}{1-\upsilon^2}\left[-z\upsilon\frac{\partial^2 w}{\partial r^2}-\frac{z}{r}\frac{\partial w}{\partial r}-\alpha_5\left(\varepsilon_1+\sum_{n=1}^{N}\frac{\tau_1^n}{n!}\frac{\partial^n}{\partial t^n}\right)\varphi\right], \tag{38}$$

where

$$\alpha_1=\frac{24\alpha_T T_0(1+\upsilon)}{\pi^2 h},\ \alpha_2=\frac{12\left(1-\upsilon^2\right)}{h^2},\ \alpha_3=\frac{K^*}{c_0^2\eta K},\ \alpha_4=\frac{\alpha_T Ez}{\eta K(1-2\nu)\sin(pz)},\ \alpha_5=\alpha_T(1+\upsilon)T_0.$$

and $\alpha_4\big|_{z=0}=\lim_{z\to 0}\left(\dfrac{\alpha_T Ez}{\eta K(1-2\nu)\sin(pz)}\right)=\dfrac{E\alpha_T}{K\eta(1-2\upsilon)}\lim_{z\to 0}\left(\dfrac{z}{\sin(pz)}\right)=\dfrac{E\alpha_T}{K\eta(1-2\upsilon)p}$.

The primes are removed for simplicity.

The Laplace transform, which is defined as follows, will be applied:

$$\overline{f}\left(r,s\right)=\int_0^\infty e^{-st}\ f\left(r,t\right)dt\ . \tag{39}$$

The initial conditions are given as follows:

$$\vartheta\left(r,t\to 0^+\right)=w\left(r,t\to 0^+\right)=\frac{\partial^n\vartheta\left(r,t\to 0^+\right)}{\partial t^n}=\frac{\partial^n w\left(r,t\to 0^+\right)}{\partial t^n},\ n\geq 1\,. \tag{40}$$

After using the Laplace transform, we get:

$$\nabla^2\nabla^2\overline{w}+\beta_1\nabla^2\overline{\vartheta}+\beta_2\overline{w}=0\,, \tag{41}$$

$$\left(\nabla^2-p^2\right)\overline{\vartheta}=\beta_3\overline{\vartheta}-\beta_4\nabla^2\overline{w}\,, \tag{42}$$

$$\overline{\sigma}_{rr}=\frac{1}{1-\upsilon^2}\left[-z\frac{\partial^2\overline{w}}{\partial r^2}-\frac{\upsilon z}{r}\frac{\partial\overline{w}}{\partial r}-\beta_5\overline{\varphi}\right], \tag{43}$$

$$\overline{\sigma}_{\theta\theta}=\frac{1}{1-\upsilon^2}\left[-z\upsilon\frac{\partial^2\overline{w}}{\partial r^2}-\frac{z}{r}\frac{\partial\overline{w}}{\partial r}-\beta_5\overline{\varphi}\right], \tag{44}$$

$$\overline{\varepsilon}_{rr}=-z\frac{\partial^2\overline{w}}{\partial r^2},\quad \overline{\varepsilon}_{\theta\theta}=-z\frac{1}{r}\frac{\partial\overline{w}}{\partial r}, \tag{45}$$

and

$$\overline{\varepsilon}=-z\nabla^2\overline{w}\,, \tag{46}$$

where $\beta_1=\alpha_1\left(\varepsilon_1+\sum_{n=1}^{N}\frac{\tau_1^n}{n!}s^n\right)$, $\beta_2=\alpha_2 s^2$, $\beta_3=\frac{s^2\left(1+\tau_q s\right)}{\left(s+\alpha_3\right)}\left(\varepsilon_1+\sum_{n=1}^{N}\frac{\tau_1^n}{n!}s^n\right)$,

$\beta_4=\frac{s^2\left(1+\tau_q s\right)\alpha_4}{\left(s+\alpha_3\right)}\left(\varepsilon_2+\sum_{m=1}^{M}\frac{\tau_2^{m-1}}{(m-1)!}s^{m-1}\right)$, $\beta_5=\alpha_5\left(\varepsilon_1+\sum_{n=1}^{N}\frac{\tau_1^n}{n!}s^n\right)$.

Equations (41) and (42) give:

$$\left(\nabla^2\nabla^2+\beta_2\right)\overline{w}+\beta_1\nabla^2\overline{\vartheta}=0\,, \tag{47}$$

and

$$\beta_4\nabla^2\overline{w}+\left(\nabla^2-\beta_6\right)\overline{\vartheta}=0\,. \tag{48}$$

where $\beta_6=p^2+\beta_3$

By eliminating between equations (47) and (48), we get the following ordinary differential equations:

$$\left(\nabla^6-\ell_1\nabla^4+\ell_2\nabla^2-\ell_3\right)\left\{\overline{w},\overline{\vartheta}\right\}=0\,, \tag{49}$$

where $\ell_1 = \beta_6 + \beta_1\beta_4,\ \ \ell_2 = \beta_2,\ \ \ell_3 = \beta_6\beta_2$.

The bounded solutions of the ordinary differential equations (49) take the following forms:

$$\bar{\vartheta}(r,s) = \sum_{i=1}^{3} A_i I_0(k_i r), \tag{50}$$

and

$$\bar{w}(r,s) = \sum_{i=1}^{3} B_i I_0(k_i r), \tag{51}$$

where $I_0(*)$ is the well-known modified Bessel functions of the first kind of order zero, and $\pm k_1, \pm k_2, \pm k_3$ are the roots of the characteristic equation:

$$\left(\nabla^2 - k_1^2\right)\left(\nabla^2 - k_2^2\right)\left(\nabla^2 - k_3^2\right)\left\{\bar{w}, \bar{\vartheta}\right\} = 0. \tag{52}$$

Hence, from the equation (48), we have:

$$B_i = -\frac{\left(k_i^2 - \beta_6\right)}{\beta_4 k_i^2} A_i. \tag{53}$$

Then, we obtain:

$$\bar{w}(r,s) = -\frac{1}{\beta_4}\sum_{i=1}^{3} \frac{\left(k_i^2 - \beta_6\right)}{k_i^2} A_i I_0(k_i r). \tag{54}$$

A supported circular micro-plate will be considered when it is thermally loaded on the bounding plane $r = a$ [29]:

$$w(a,t) = \nabla^2 w(r,t)\big|_{r=a} = 0, \tag{55}$$

and

$$\vartheta(a,t) = \vartheta_o \omega(t). \tag{56}$$

Applying the Laplace transform to the above conditions, we obtain:

$$\bar{w}(a,s) = \nabla^2 \bar{w}(r,s)\big|_{r=a} = 0, \tag{57}$$

and

$$\vartheta(a,s) = \vartheta_0 \bar{\omega}(s). \tag{58}$$

where ϑ_0 gives the thermal loading intensity, which is constant.

By applying the boundary conditions in (50) and (51), we get the following linear system of equations:

$$\sum_{i=1}^{3} A_i I_0\left(k_i a\right) = \vartheta_0 \bar{\omega}(s), \tag{59}$$

$$\sum_{i=1}^{3} \frac{\left(k_i^2 - \beta_6\right)}{k_i^2} A_i I_0\left(k_i a\right) = 0, \tag{60}$$

and

$$\sum_{i=1}^{3} \left(k_i^2 - \beta_6\right) A_i I_0\left(k_i a\right) = 0. \tag{61}$$

Solving the system in (59)-(61), gives the solutions of the parameters A_1, A_2, A_3, hence, the solutions of the studied functions in the Laplace transform domain are as follows:

$A_1 = \dfrac{\vartheta_0 \bar{\omega}(s) k_1^2 \left(k_2^2 - \beta_6\right)\left(k_3^2 - \beta_6\right)}{\beta_6 \left(k_1^2 - k_3^2\right)\left(k_1^2 - k_2^2\right) I_0\left(k_1 a\right)}$, $A_2 = \dfrac{\vartheta_0 \bar{\omega}(s) k_2^2 \left(k_1^2 - \beta_6\right)\left(k_3^2 - \beta_6\right)}{\beta_6 \left(k_2^2 - k_3^2\right)\left(k_2^2 - k_1^2\right) I_0\left(k_2 a\right)}$, and

$A_3 = \dfrac{\vartheta_0 \bar{\omega}(s) k_3^2 \left(k_1^2 - \beta_6\right)\left(k_2^2 - \beta_6\right)}{\beta_6 \left(k_3^2 - k_1^2\right)\left(k_3^2 - k_2^2\right) I_0\left(k_3 a\right)}$.

Thus, the final solution $\bar{\varphi}(r,z,s)$ in the Laplace transform domain of the temperature increment function is given as:

$$\bar{\varphi}(r,z,s) = \frac{\vartheta_0\, \bar{\omega}(s) \sin(p z)}{\beta_6} \left(\begin{array}{c} \dfrac{k_1^2 \left(k_2^2 - \beta_6\right)\left(k_3^2 - \beta_6\right) I_0\left(k_i r\right)}{\left(k_1^2 - k_3^2\right)\left(k_1^2 - k_2^2\right) I_0\left(k_1 a\right)} + \\ \dfrac{k_2^2 \left(k_3^2 - \beta_6\right)\left(k_1^2 - \beta_6\right) I_0\left(k_2 r\right)}{\left(k_2^2 - k_1^2\right)\left(k_2^2 - k_3^2\right) I_0\left(k_2 a\right)} + \\ \dfrac{k_3^2 \left(k_1^2 - \beta_6\right)\left(k_2^2 - \beta_6\right) I_0\left(k_3 r\right)}{\left(k_3^2 - k_1^2\right)\left(k_3^2 - k_2^2\right) I_0\left(k_3 a\right)} \end{array} \right) \tag{62}$$

and the final solution of the vibration function or the vibration of the micro-plate $\bar{w}(r,s)$ in the Laplace transform domain is as follows:

$$\bar{w}(r,s) = \vartheta_0\, \bar{\omega}(s) \beta_1 \beta_4 \beta_6 \left[\begin{array}{c} \dfrac{I_0\left(k_1 r\right)}{\left(k_1^2 - k_3^2\right)\left(k_1^2 - k_2^2\right) I_0\left(k_1 a\right)} + \\ \dfrac{I_0\left(k_2 r\right)}{\left(k_2^2 - k_3^2\right)\left(k_2^2 - k_3^2\right) I_0\left(k_2 a\right)} + \\ \dfrac{I_0\left(k_3 r\right)}{\left(k_3^2 - k_1^2\right)\left(k_3^2 - k_2^2\right) I_0\left(k_3 a\right)} \end{array} \right] \tag{63}$$

From the equations (46) and (63), we have the final solution of the volumetric dilatation function:

$$\bar{\varepsilon}\left(r,z,s\right)=-z\vartheta_0\,\bar{\omega}\left(s\right)\beta_1\beta_4\beta_6\left[\begin{array}{c}\dfrac{k_1^2 I_0\left(k_1 r\right)}{\left(k_1^2-k_3^2\right)\left(k_1^2-k_2^2\right)I_0\left(k_1 a\right)}+\\ \dfrac{k_2^2 I_0\left(k_2 r\right)}{\left(k_2^2-k_3^2\right)\left(k_2^2-k_3^2\right)I_0\left(k_2 a\right)}+\\ \dfrac{k_3^2 I_0\left(k_3 r\right)}{\left(k_3^2-k_1^2\right)\left(k_3^2-k_2^2\right)I_0\left(k_3 a\right)}\end{array}\right] \tag{64}$$

As a function of the thermal loading on the boundary plane of the micro-plate, we assume that the ramp-type heat source with a parameter $t_0 \neq 0$ is applied to the circular micro-plate in the following form:

$$\omega\left(t\right)=\left\{\begin{array}{ll}\dfrac{t}{t_0} & 0<t<t_0\\ 1 & t\geq t_0\end{array}\right\} \tag{65}$$

which gives, after applying the Laplace transform, the following form:

$$\bar{\omega}\left(s\right)=\frac{1-e^{-st_0}}{s^2 t_0} \tag{66}$$

It is available to obtain the average stress distribution as follows:

$$\bar{\sigma}\left(r,z,s\right)=\frac{\bar{\sigma}_{rr}+\bar{\sigma}_{\theta\theta}}{2}=\frac{1}{2\left(1-\upsilon\right)}\bar{\varepsilon}\left(r,z,s\right)-\frac{\beta_5}{\left(1-\upsilon^2\right)}\bar{\varphi}\left(r,z,s\right) \tag{67}$$

Numerical results and discussion

A circular silicon microplate is assumed in the following numerical calculations. Here are the mechanical and thermal properties [4], [29][14,26,27,44,58-61]:

$K=141.04\,\mathrm{W/(mK)}$, $C_E=1.64\times10^6\,\mathrm{J/(kgK)}$, $\alpha_T=2.6\times10^{-6}\,\mathrm{K^{-1}}$, $\rho=2330\ \mathrm{kg/m^3}$, $T_0=300\,\mathrm{K}$, $E_0=165.0\ \mathrm{GPa}$, $\tau_q=6.7\times10^{-12}\,\mathrm{s}$, $\upsilon=0.22$.

The inverse of the Laplace transform can be calculated by applying the Riemann-sum approximation method [46]:

$$f\left(r,t\right)=\frac{e^{\kappa t}}{t}\left[\frac{1}{2}\bar{f}\left(r,\kappa\right)+\mathrm{Re}\sum_{j=1}^{J}\left(-1\right)^j\bar{f}\left(r,\kappa+\frac{i\,j\pi}{t}\right)\right], \tag{68}$$

where "$i=\sqrt{-1}$" is an imaginary number unit, and "Re" is the real part, and for faster convergence, the value κ satisfies the relation $\kappa t\approx4.7$.

By inputting formula (68) into the MAPLE software, we can easily compute the inverse Laplace transform. For the dimensionless parameter, the findings have been classified into six groups to illustrate the temperature rise, vibration, volumetric expansion, and mean stress, respectively, across a wide range of $r\left(0 \le r \le 3\right)$ conditions.

The temperature increment distributions for the seven analyzed models, as seen in Figures 2-13, display analogous patterns and are quite comparable. The transmission of thermal waves throughout the seven analyzed models is consistent, with little deviations among them. This outcome is anticipated at the micro- and nano-scale inside resonators. The variations in vibration, volumetric expansion, and mean stress across the seven examined models exhibit differences in both magnitude and behavior. The transmission of mechanical waves varies across various models.

In illustrations 3, 7, and 11, depicting the vibration dispersion, the disparities across the seven examined models are evident. The G-N-I distribution has four peak points, in contrast to all other models which include three, each differing in values and positions.

The maximum values of the vibrations have the following order:

$$\left|w_{\text{G-N-I}}^{\text{Max}}\right| > \left|w_{\text{S-G-L}}^{\text{Max}}\right| > \left|w_{\text{CTE}}^{\text{Max}}\right| > \left|w_{\text{L-S}}^{\text{Max}}\right| > \left|w_{\text{R-G-L}}^{\text{Max}}\right| > \left|w_{\text{M-G-T}}^{\text{Max}}\right| > \left|w_{\text{G-N-III}}^{\text{Max}}\right|. \tag{69}$$

In Figures 4, 8, and 12, depicting the volumetric dilatation distribution, variances across the seven examined models are evident. The G-N-I distribution has four peak points, whereas all other models exhibit three, differing in both values and positions.

The maximum values of the volumetric dilatation have the following order:

$$\left|\varepsilon_{\text{G-N-I}}^{\text{Max}}\right| > \left|\varepsilon_{\text{S-G-L}}^{\text{Max}}\right| > \left|\varepsilon_{\text{CTE}}^{\text{Max}}\right| > \left|w_{\text{G-N-III}}^{\text{Max}}\right| > \left|w_{\text{M-G-T}}^{\text{Max}}\right| > \left|w_{\text{L-S}}^{\text{Max}}\right| > \left|w_{\text{R-G-L}}^{\text{Max}}\right|. \tag{70}$$

In figures 5, 9, and 13, depicting the mean stress distribution, the disparities across the seven analyzed models are evident. The G-N-I distribution has five peaks, whereas all other models have two, differing in both values and positions.

The absolute value of the average stress on the bounding plane of the plate surface $r = a$ has the following order:

$$\left|\sigma_{\text{G-N-I}}^{\text{r=a}}\right| > \left|\sigma_{\text{S-G-L}}^{\text{r=a}}\right| > \left|\sigma_{\text{G-N-I}}^{\text{r=a}}\right| > \left|\sigma_{\text{CTE}}^{\text{r=a}}\right| > \left|\sigma_{\text{G-N-III}}^{\text{r=a}}\right| > \left|\sigma_{\text{M-G-T}}^{\text{r=a}}\right| > \left|\sigma_{\text{L-S}}^{\text{r=a}}\right|. \tag{71}$$

It is evident that the Green-Naghdi Type-III and Moore–Gibson–Thompson models exhibit the most similar mechanical behavior, followed by the Biot model of linked thermoelasticity and the Lord-Sulman model of generalized thermoelasticity.The data shown in figures 2-13 has

been classified into three distinct categories. These groups illustrate the distributions of temperature increase, vibration, volumetric expansion, and mean stress, respectively.

The first group of figures contains Figures 2-5 for two different values of the ramp-time heat parameter when $t = t_0$ and $t < t_0$ showing the effect of this parameter on the studied functions under the seven studied models.

Figures 2a and 2b illustrate that the ramp-time heat parameter substantially influences the distributions of temperature increases, where higher ramp-time heat parameters result in diminished temperature increments throughout the seven analyzed models.

Figures 3a and 3b illustrate that the ramp-time heat parameter considerably influences the vibration distributions, with a rise in the ramp-time heat parameter correlating to an increase in the absolute value of vibration throughout the seven examined models.

Figures 4a and 4b illustrate that the ramp-time heat parameter substantially influences the distributions of volumetric dilatation, with an elevation in the ramp-time heat parameter resulting in a greater absolute value of volumetric dilatation throughout the seven examined models.

Figures 5a and 5b illustrate that the ramp-time heat parameter substantially influences the distributions of average stress, with an elevation in the ramp-time heat parameter resulting in a reduction in the absolute value of average stress throughout the seven examined models.

The second group of figures contains Figures 6-9 for two different values of the plate thickness parameter when $h = a/6.0$ and $h = a/8.0$ to examine the effect of this parameter on the studied functions under the seven studied models.

Figures 6a and 6b illustrate that the parameter of plate thickness substantially influences the temperature increment distributions, where diminished values result in reduced temperature increases throughout the seven models examined.

Figures 7a and 7b illustrate that the parameter of plate thickness substantially influences the vibration distributions, wherein a reduction in this parameter results in an escalation of the absolute vibration values throughout the seven models examined.

Figures 8a and 8b illustrate that the parameter of plate thickness considerably influences the volumetric dilatation distributions, with a reduction in the plate thickness parameter correlating to an elevation in the absolute volumetric dilatation across the seven models examined.

Figures 9a and 9b illustrate that the parameter of plate thickness considerably influences the average stress distribution, with reduced plate thickness resulting in elevated absolute values of average stress throughout the seven examined models.

The third group of figures contains Figures 10-13 for two different values of z when $z = h/4$ and $z = h/3$ to examine the impact of this parameter on the studied functions across the seven models.

Figures 10a and 10b illustrate that the parameter z substantially influences the temperature increment distributions, with a rise in the parameter z correlating with an increase in the temperature increment throughout the seven examined models.Figures 11a and 11b illustrate that the parameter z has no influence on the vibration distributions.Figures 12a and 12b illustrate that the parameter z substantially influences the volumetric dilatation distributions, with higher values of z resulting in an increased absolute volumetric dilatation throughout the seven analyzed models.Figures 13a and 13b illustrate that the parameter z substantially influences the distributions of the mean stress, with a rise in the parameter z correlating with an increase in the absolute magnitude of the mean stress throughout the seven examined models.

Conclusion

This study developed a unified mathematical formulation to investigate the thermoelastic vibration behavior of a supported circular silicon microplate within the framework of seven different thermoelasticity theories based on the Kirchhoff–Love plate model. The proposed formulation enabled a systematic comparative analysis of the thermomechanical responses predicted by the refined Green–Lindsay, Biot, Lord–Shulman, Green–Naghdi Type-I, Green–Naghdi Type-III, simple Green–Lindsay, and Moore–Gibson–Thompson models under identical physical and geometric conditions. The analytical solutions were successfully obtained using the Laplace transform technique, and the transient responses were evaluated numerically through an efficient inversion procedure.

The results demonstrate that the distributions of temperature increments predicted by the seven thermoelastic models exhibit very similar behaviour, indicating that the propagation of thermal waves in silicon microplate resonators is nearly identical across the considered theories.

In contrast, noticeable differences were observed in the mechanical responses, including vibration, volumetric dilatation, and stress distributions, confirming the sensitivity of mechanical wave propagation to the adopted thermoelastic model.

In particular, the Green–Naghdi Type-III and Moore–Gibson–Thompson models were found to exhibit the closest mechanical behavior, followed by the Biot and Lord–Shulman models, highlighting their relative consistency in predicting dynamic responses. These observations are consistent with the numerical comparisons presented in the study.

Furthermore, the parametric analysis revealed that the ramp-time heating parameter, plate thickness, and spatial position along the thickness direction significantly influence the microplate's thermomechanical characteristics. Increasing the ramp-time parameter was shown to modify the amplitude of vibration, deformation, and stress, while variations in plate thickness strongly affected the magnitude of the mechanical responses. These findings confirm that geometric and thermal parameters play a critical role in controlling the dynamic behavior of micro-scale thermoelastic structures.

Overall, the proposed unified framework provides a comprehensive, flexible tool for evaluating the relative performance of multiple thermoelastic models within a single, consistent formulation.

The results of this study contribute to a deeper understanding of thermomechanical wave propagation in micro- and nanoscale resonators and offer practical guidance for the design, optimization, and thermal management of advanced microelectromechanical systems (MEMS) and nanoelectromechanical systems (NEMS).

Institutional Review Board Statement: Not applicable.

Data Availability Statement: The authors declare that the paper has no data to share.

Conflicts of Interest: The authors declare no competing interests.

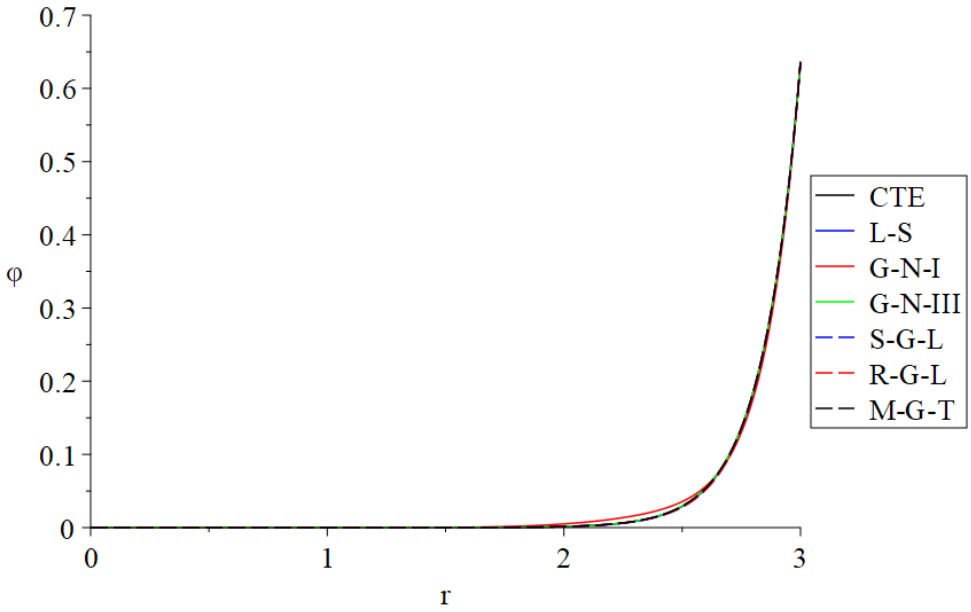


Figure 2a: The temperature increments when $t_0 = t$

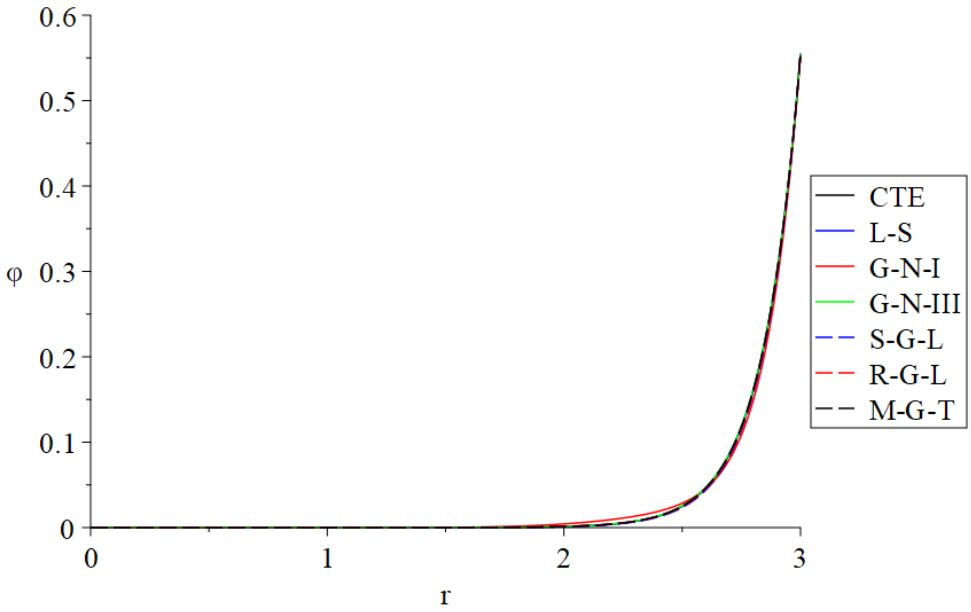


Figure 2b: The temperature increments when $t_0 > t$

Figure 2: The temperature increments under the studied theorems and different values of ramp-time heat parameter t_0

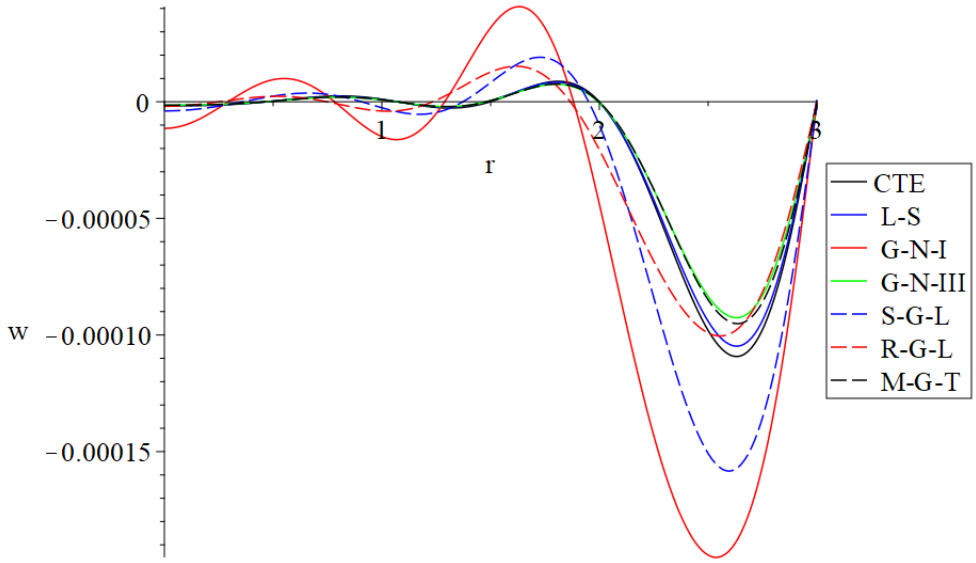


Figure 3a: The vibration when $t_0 = t$

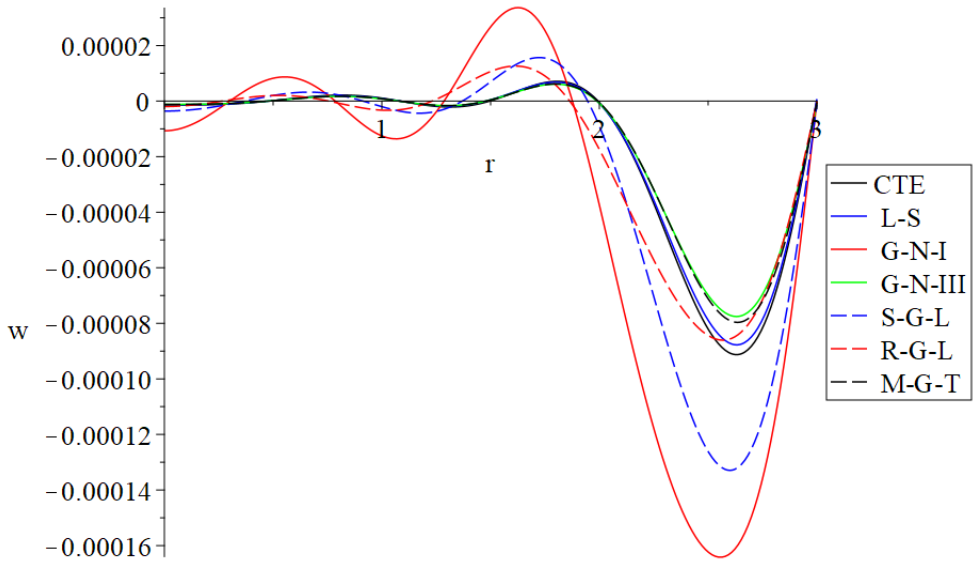


Figure 3b: The vibration when $t_0 > t$

Figure 3: The vibration under the studied theorems and different values of ramp-time heat parameter t_0

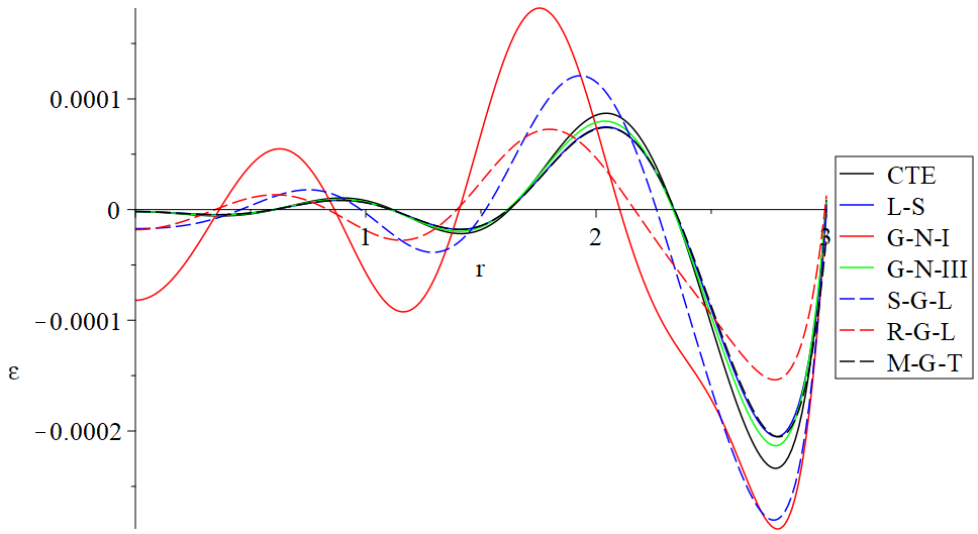


Figure 4a: The volumetric dilatation when $t_0 = t$

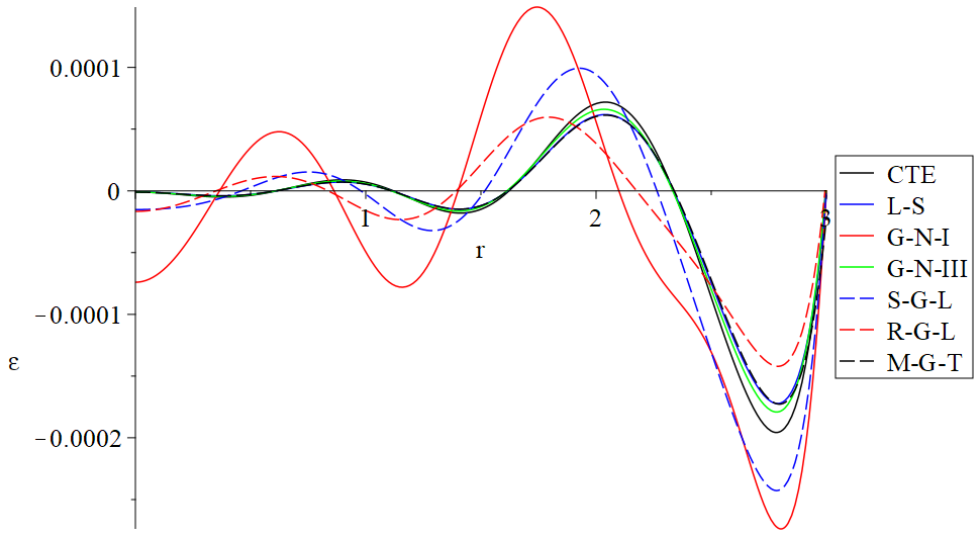


Figure 4b: The volumetric dilatation when $t_0 > t$

Figure 4: The volumetric dilatation under the studied theorems and different values of ramp-time heat parameter t_0

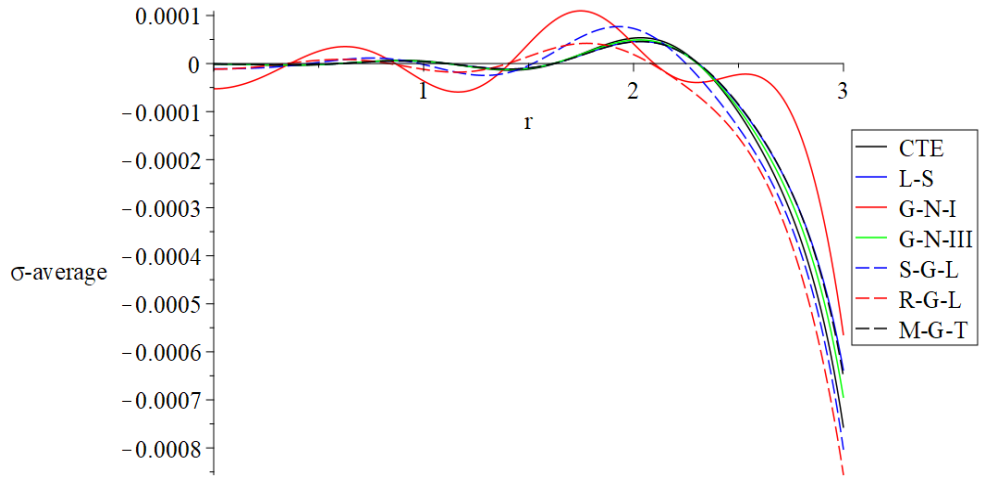


Figure 5a: The average stress when $t_0 = t$

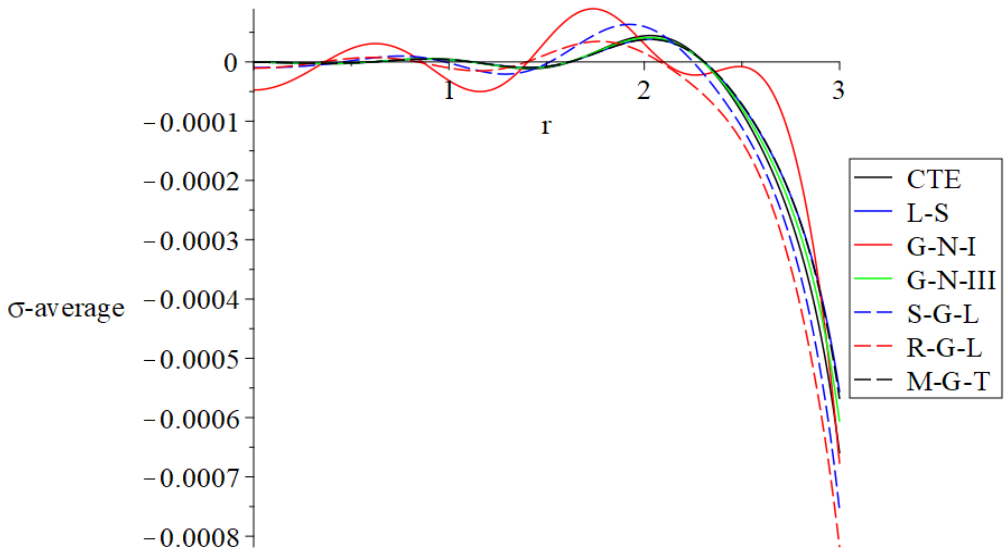


Figure 5b: The average stress when $t_0 > t$

Figure 5: The average stress under the studied theorems and different values of ramp-time heat parameter t_0

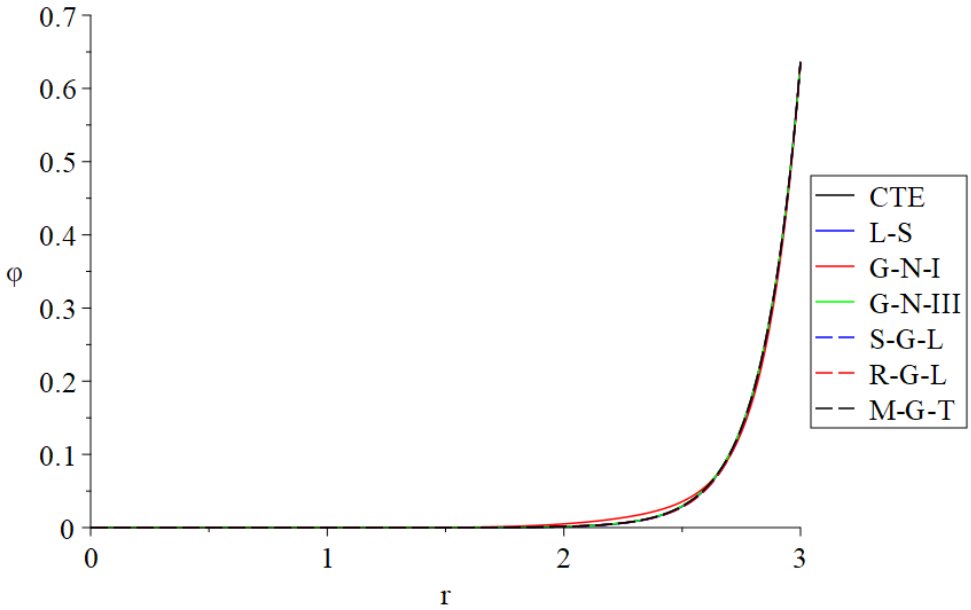


Figure 6a: The temperature increments when $h = a / 6.0$

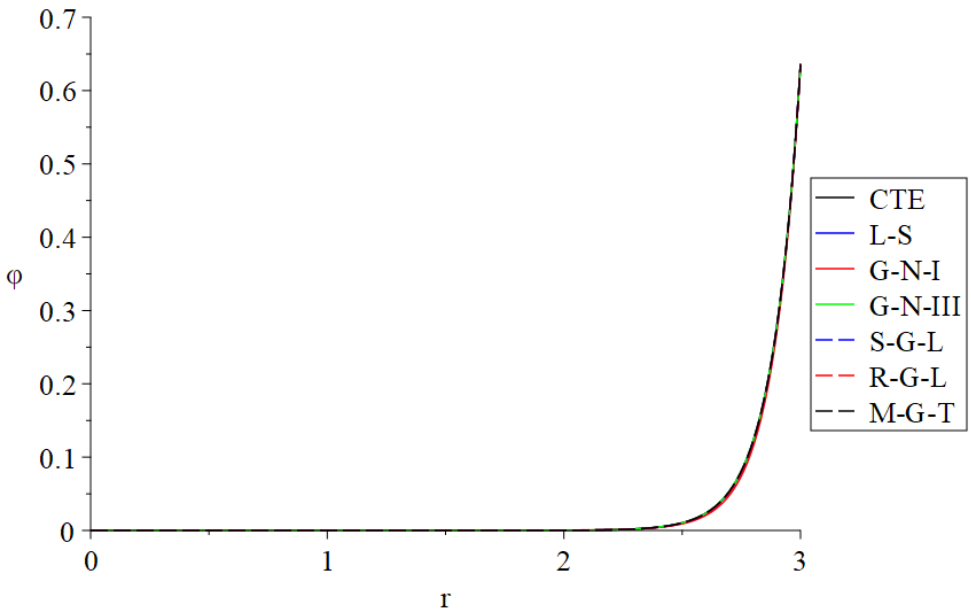


Figure 6b: The temperature increments when $h = a / 8.0$

Figure 6: The temperature increments under the studied theorems and different values of plate thickness parameter h

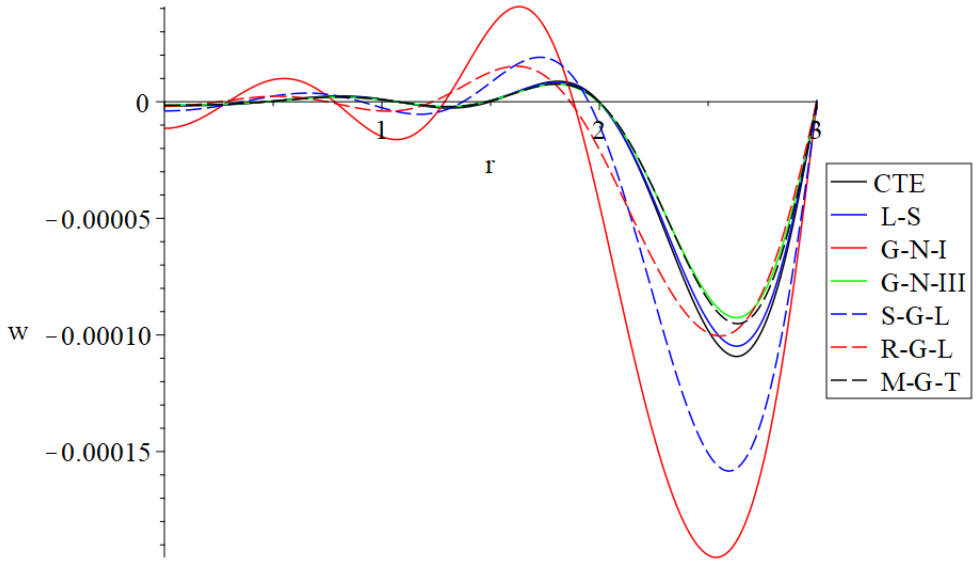


Figure 7a: The vibration when $h = a / 6.0$

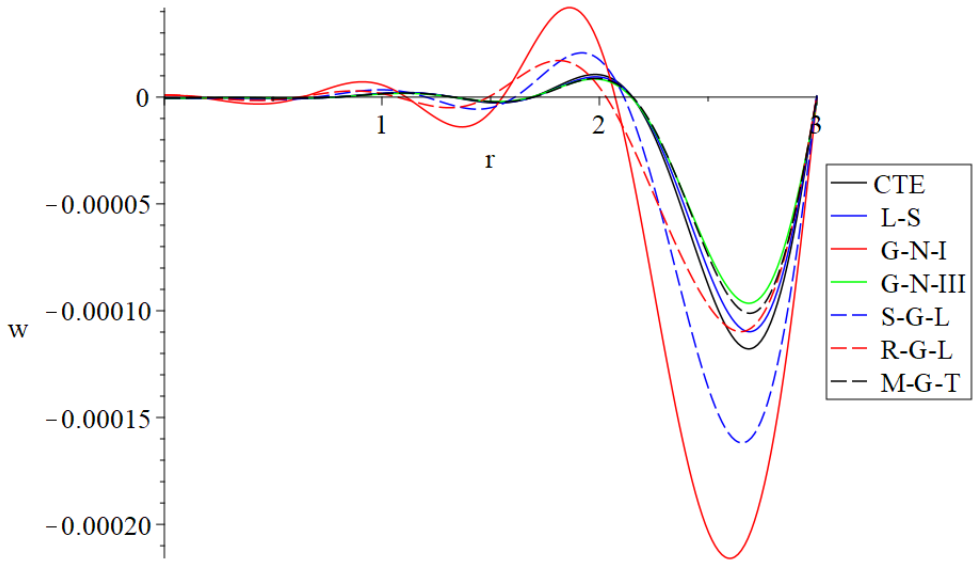


Figure 7b: The vibration when $h = a / 8.0$

Figure 7: The vibration under the studied theorems and different values of plate thickness parameter h

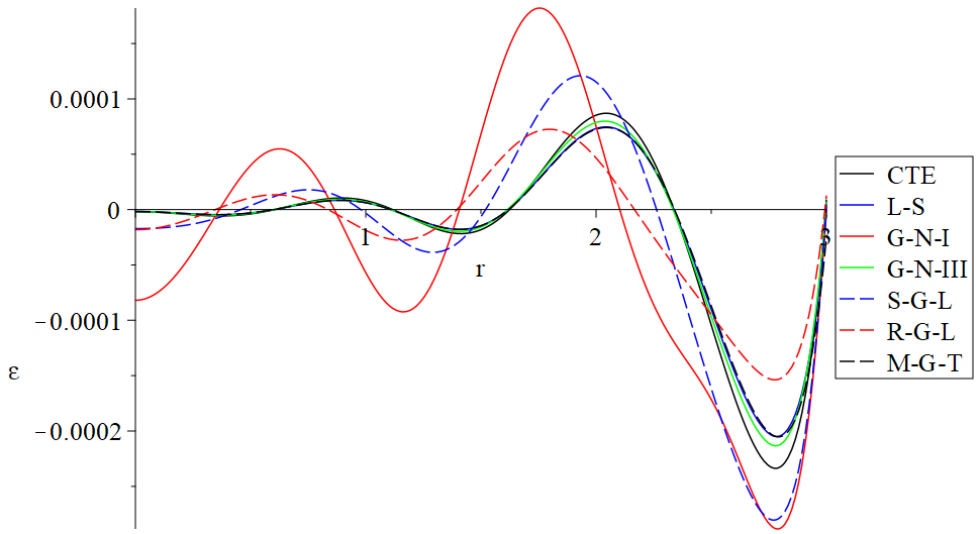


Figure 8a: The volumetric dilatation when $h = a/6.0$

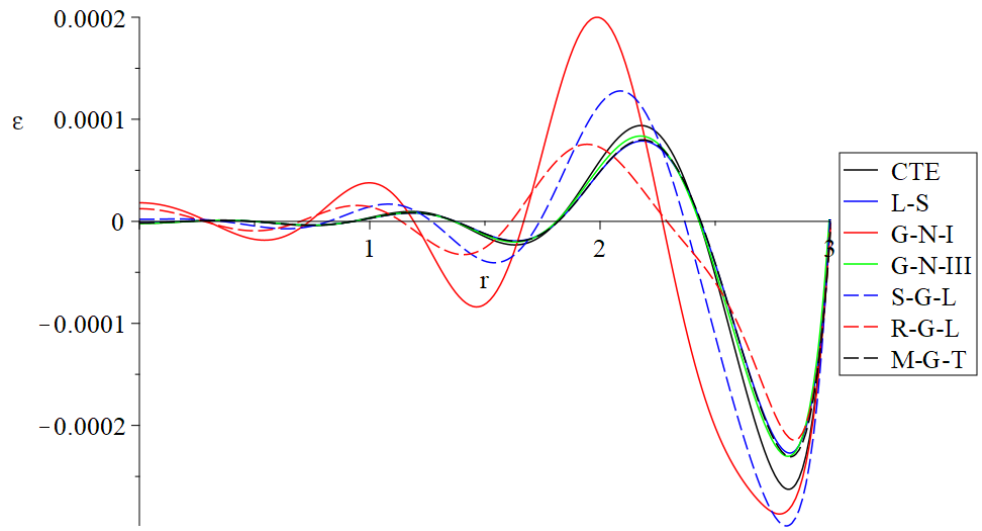


Figure 8b: The volumetric dilatation when $h = a/8.0$

Figure 8: The volumetric dilatation under the studied theorems and different values of plate thickness parameter h

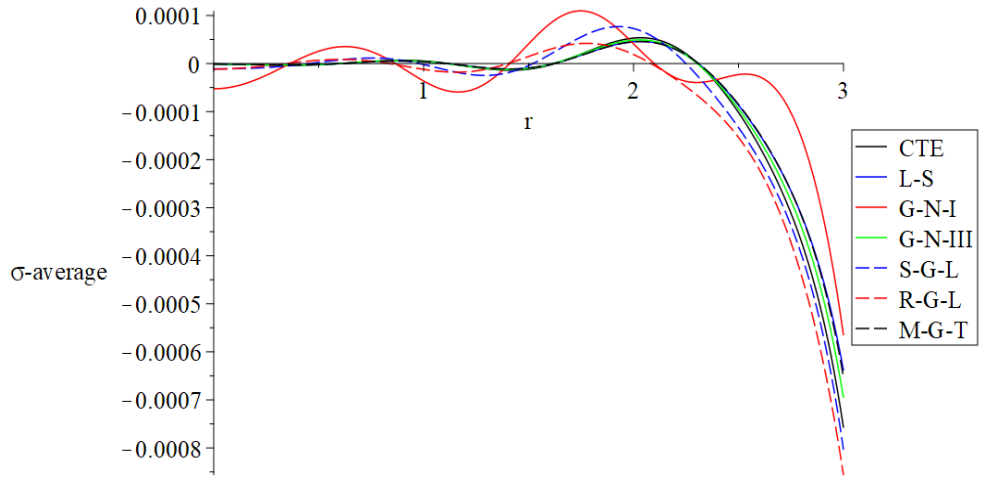


Figure 9a: The average stress when $h = a/6.0$

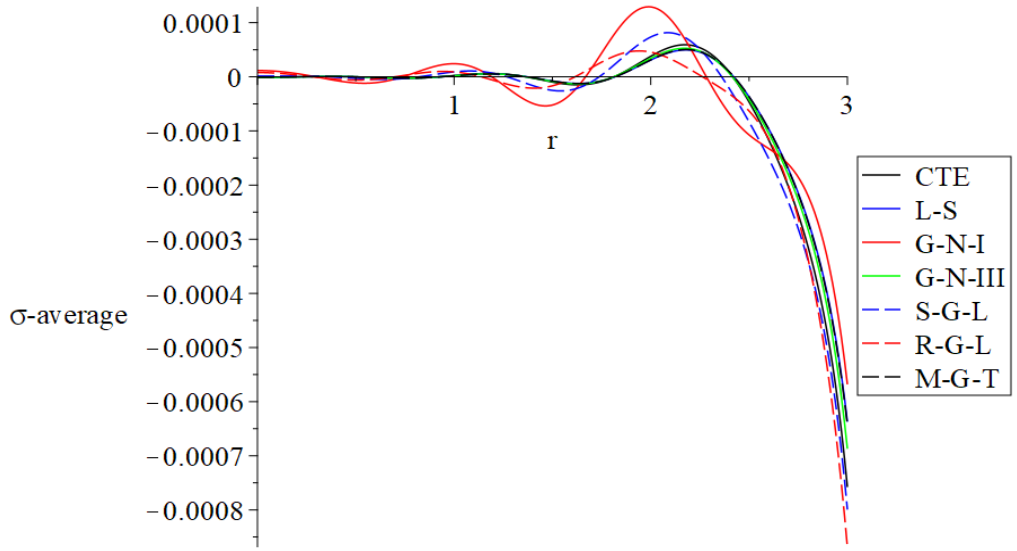


Figure 9b: The average stress when $h = a/8.0$

Figure 9: The average stress under the studied theorems and different values of plate thickness parameter h

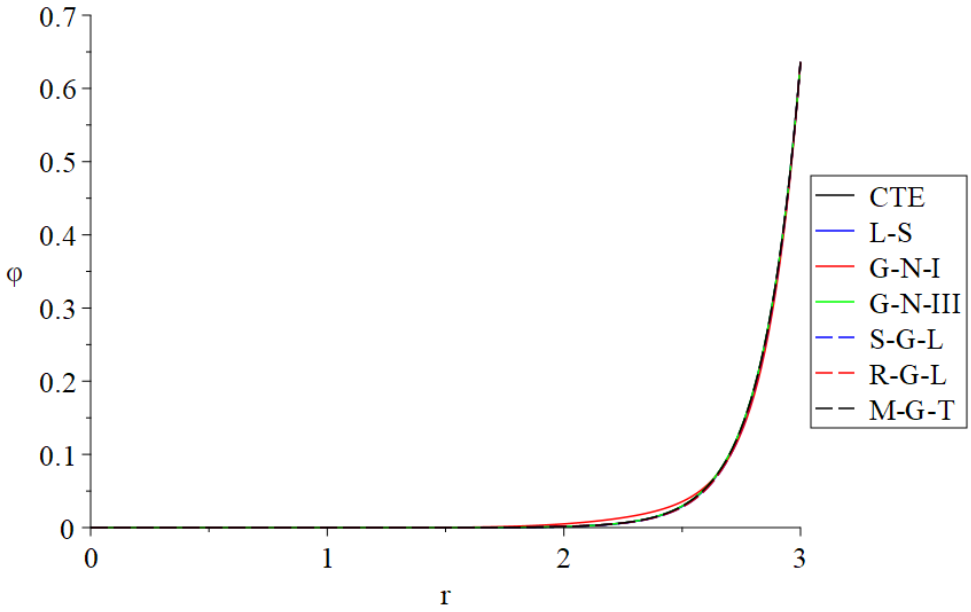


Figure 10a: The temperature increments when $z = h/4$

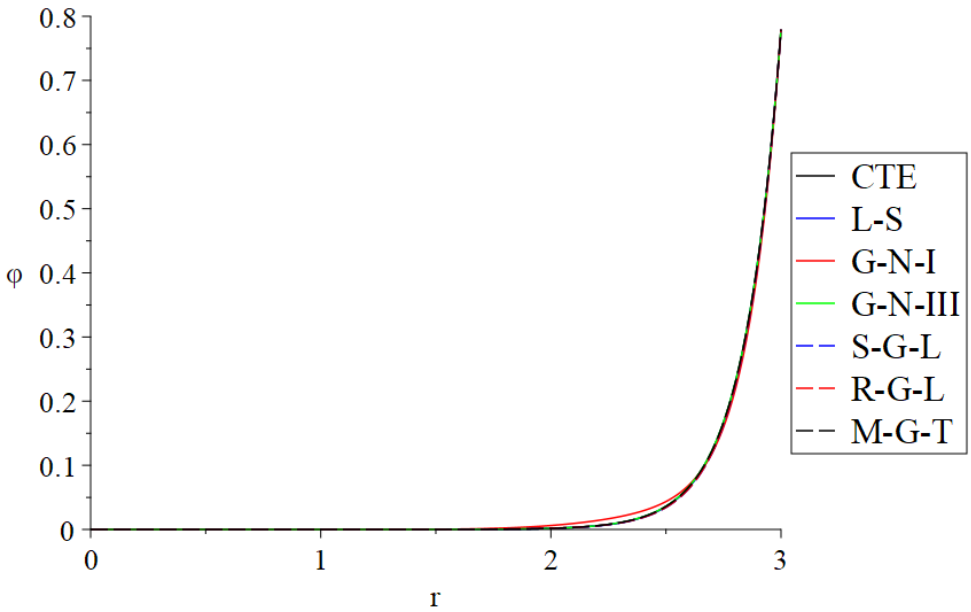


Figure 10b: The temperature increments when $z = h/3$

Figure 10: The temperature increments under the studied theorems and different values of z

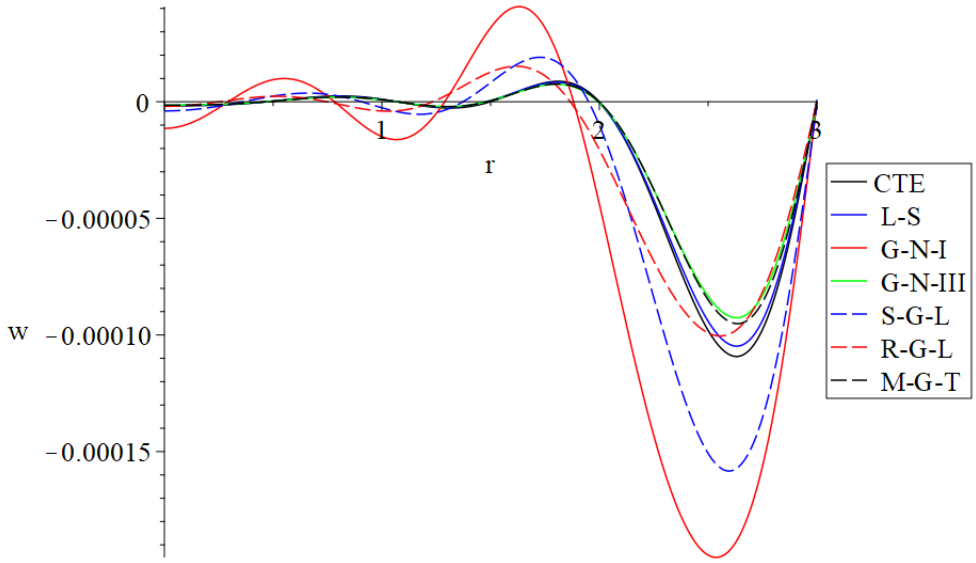


Figure 11a: The vibration when $z = h/4$

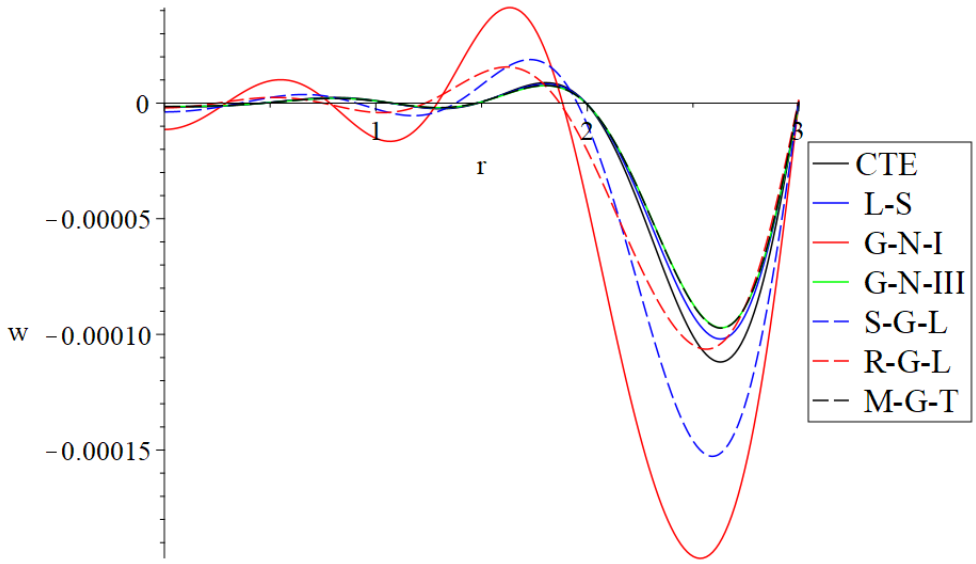


Figure 11b: The vibration when $z = h/3$

Figure 11: The vibration under the studied theorems and different values of z

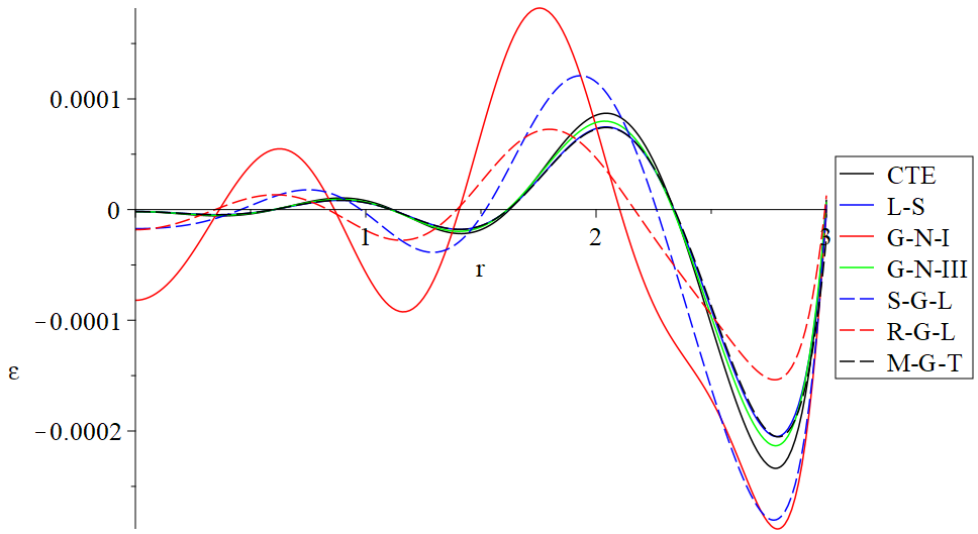


Figure 12a: The volumetric dilatation when $z = h/4$

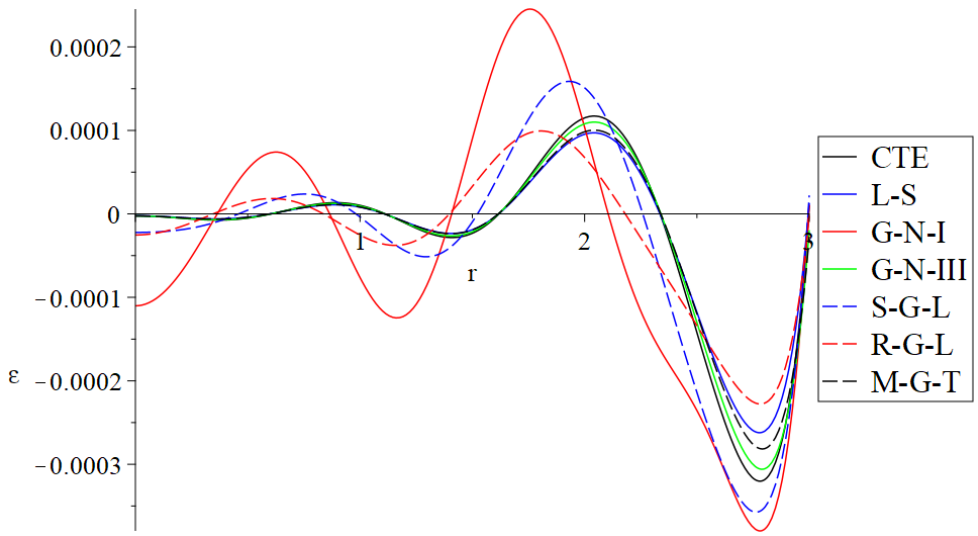


Figure 12b: The volumetric dilatation when $z = h/3$

Figure 12: The volumetric dilatation under the studied theorems and different values of z

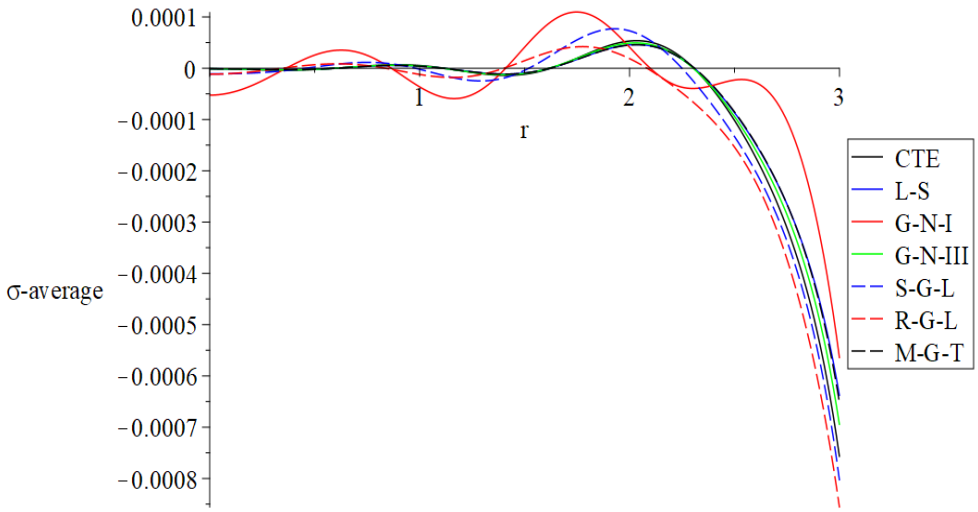


Figure 13a: The average stress when $z = h/4$

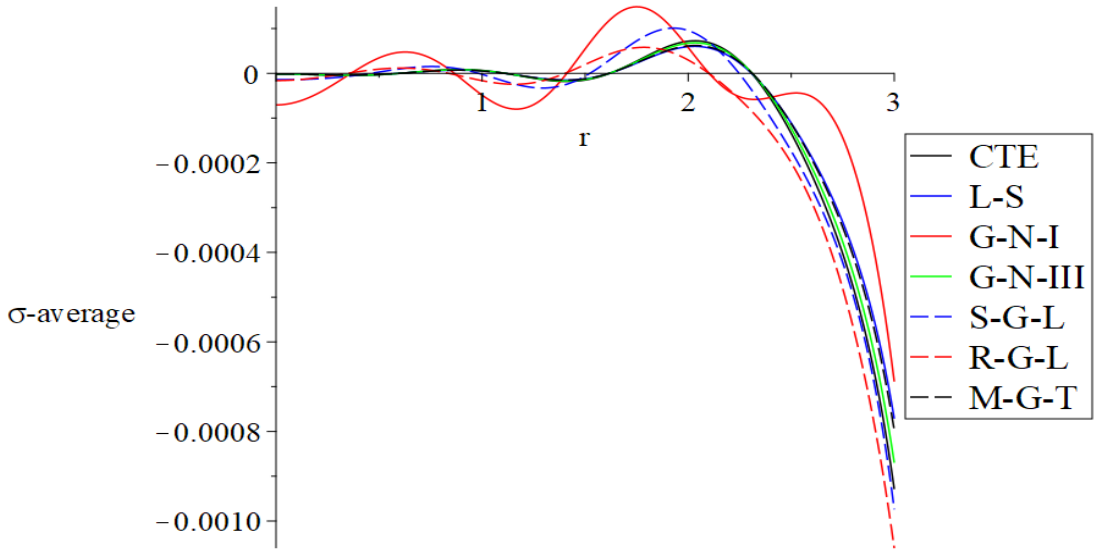


Figure 13b: The average stress when $z = h/3$

Figure 13: The average stress under the studied theorems and different values of z

References

[1] Hao Z. Thermoelastic damping in the contour-mode vibrations of micro-and nano-electromechanical circular thin-plate resonators. Journal of Sound and Vibration. 2008;313(1-2):77-96.

[2] Sun Y, Tohmyoh H. Thermoelastic damping of the axisymmetric vibration of circular plate resonators. Journal of sound and vibration. 2009;319(1-2):392-405.

[3] Sun Y, Saka M. Thermoelastic damping in micro-scale circular plate resonators. Journal of Sound and Vibration. 2010;329(3):328-337.

[4] Grover D. Damping in thin circular viscothermoelastic plate resonators. Canadian Journal of Physics. 2015;93(12):1597-1605.

[5] Grover D. Clamped-free micro-scale transversely isotropic thermoelastic beam resonators. Microsystem Technologies. 2019:1-8.

[6] Grover D, Seth R. Generalized viscothermoelasticity theory of dual-phase-lagging model for damping analysis in circular micro-plate resonators. Mechanics of Time-Dependent Materials. 2019;23(1):119-132.

[7] Guo F, Song J, Wang G, et al. Analysis of thermoelastic dissipation in circular micro-plate resonators using the generalized thermoelasticity theory of dual-phase-lagging model. Journal of Sound and Vibration. 2014;333(11):2465-2474.

[8] Guo F, Wang G, Rogerson G. Analysis of thermoelastic damping in micro-and nanomechanical resonators based on dual-phase-lagging generalized thermoelasticity theory. International Journal of Engineering Science. 2012;60:59-65.

[9] Biot MA. Thermoelasticity and Irreversible Thermodynamics. J Appl Phys. 1956;27(3):240-253.

[10] Sharma K, Bansal P, Gupta V. 18 Plane Wave Propagation. Manufacturing Engineering and Materials Science: Tools and Applications. 2023:194.

[11] Fadodun OO, Olokuntoye BA, Borokinni AS, et al. Thermohyperelastic constitutive response for semilinear materials with application to deformation of a rotating thin disk. Journal of Thermal Stresses. 2024;47(5):581-599.

[12] Lin X, Lyu Y, Gao J, et al. Dispersion of thermoelastic guided waves in multi-layered porous media. Mechanics of Advanced Materials and Structures. 2024:1-19.

[13] Nobili A. Hamiltonian/Stroh formalism for reversible poroelasticity (and thermoelasticity). International Journal of Solids and Structures. 2024:112935.

[14] Youssef HM, El-Bary AA. Thermoelastic Material Response Due to Laser Pulse Heating in Context of Four Theorems of Thermoelasticity. Journal of Thermal Stresses. 2014 2014/12/02;37(12):1379-1389.

[15] Lord HW, Shulman Y. A generalized dynamical theory of thermoelasticity. Journal of the Mechanics and Physics of Solids. 1967;15(5):299-309.

[16] Hetnarski RB, Ignaczak J. Generalized thermoelasticity. Journal of Thermal Stresses. 1999;22(4-5):451-476.

[17] Dhaliwal RS, Sherief HH. Generalized thermoelasticity for anisotropic media. Quarterly of Applied Mathematics. 1980;38:1-8.

[18] Kaushal S, Kumar R, Lofty K, et al. Response of frequency domain in generalized thermoelastic medium under modified Green-Lindsay with non-local and two temperature. ZAMM-Journal of Applied Mathematics and Mechanics/Zeitschrift für Angewandte Mathematik und Mechanik. 2024;104(5):e202301012.

[19] Kirti, Sahu SA. On plane wave scattering at the piezothermoelastic half-space with impedance boundary condition. Acta Mechanica. 2024:1-16.

[20] Kumari M, Rama E, Kumar R. Response of Fractional Ordered Magneto-Micropolar Thermoviscoelastic Half-Space Due To Hall Current And Rotation Under Ramp-Type Heating. Utilitas Mathematica. 2024;121:95-106.

[21] Said SM. Effect of the gravity on a nonlocal thermoelastic medium with a heat source using fractional derivative. Geomechanics and Engineering. 2024;37(6):591-597.

[22] Seth T, Mallik SH. Eringen's nonlocal elasticity theory for the analysis of two temperature generalized thermoelastic interactions in an anisotropic medium with memory. Multidiscipline Modeling in Materials and Structures. 2024;ahead-of-print(ahead-of-print).

[23] Mamatha Kumari ERRK. Response of Fractional Ordered Magneto-Micropolar Thermoviscoelastic Half- Space Due To Hall Current And Rotation Under Ramp-Type Heating. Utilitas Mathematica. 2024 07/23;121:95-106.

[24] Stelmashchuk V, Shynkarenko H. Stability of hybrid time integration scheme for Lord–Shulman thermopiezoelectricity. Results in Applied Mathematics. 2024 2024/08/01/;23:100467.

[25] Sharifi H. Magneto–thermoelastic behavior of an orthotropic hollow cylinder based on Lord–Shulman and Green–Lindsay theories. Acta Mechanica. 2024 2024/07/01;235(7):4863-4886.

[26] Abbas IA, Youssef HM. A Nonlinear Generalized Thermoelasticity Model of Temperature-Dependent Materials Using Finite Element Method. International Journal of Thermophysics. 2012 2012/07/01;33(7):1302-1313.

[27] Ezzat MA, Youssef HM. Generalized magneto-thermoelasticity in a perfectly conducting medium. International Journal of Solids and Structures. 2005 2005/12/01/;42(24):6319-6334.

[28] Müller I. The coldness, a universal function in thermoelastic bodies. Archive for Rational Mechanics and Analysis. 1971;41(5):319-332.

[29] Green AE, Laws N. On the entropy production inequality. Archive for Rational Mechanics and Analysis. 1972;45(1):47-53.

[30] Green AE, Lindsay KA. Thermoelasticity. Journal of Elasticity. 1972;2(1):1-7.

[31] Suhubi ES. Thermoelastic solids. Continuum physics. 1975;2(part 2).

[32] Kumar P, Prasad R, Kumar V, et al. Some basic theorems on the modified Green–Lindsay model of linear generalized thermoelasticity. Waves in Random and Complex Media. 2024:1-15.

[33] Kumar P, Prasad R. An investigation of the thermomechanical effects of mode-I crack under modified Green–Lindsay theory. Archive of Applied Mechanics. 2024:1-18.

[34] Sharifi H. Magneto–thermoelastic behavior of an orthotropic hollow cylinder based on Lord–Shulman and Green–Lindsay theories. Acta Mechanica. 2024:1-24.

[35] Seth T, Molla MAK, Mallik SH. Generalized Thermoelastic Interactions Using an Eigenvalue Technique in a Transversely Isotropic Unbounded Medium with Memory Having a Line Heat Source. Mechanics of Advanced Composite Structures. 2024;11(2):413-424.

[36] Zenkour AM. Thermoelastic diffusion problem for a half-space due to a refined dual-phase-lag Green-Naghdi model. Journal of Ocean Engineering and Science. 2020 2020/09/01/;5(3):214-222.

[37] Kutbi MA, Zenkour AM. Refined dual-phase-lag Green–Naghdi models for thermoelastic diffusion in an infinite medium. Waves in Random and Complex Media. 2022 2022/03/04;32(2):947-967.

[38] Mohamed MS, Lotfy K, El-Bary A, et al. Absorption illumination of a 2D rotator semi-infinite thermoelastic medium using a modified Green and Lindsay model. Case Studies in Thermal Engineering. 2021 2021/08/01/;26:101165.

[39] Zenkour AM, Saeed T, Alnefaie KM. Analysis of the Bio-Thermoelasticity Response of Biological Tissues Subjected to Harmonic Heating Using a Refined Green–Lindsay Model. Journal of Computational Applied Mechanics. 2023;54(4):588-606.

[40] Green AE, Naghdi PM. Thermoelasticity without energy dissipation. Journal of Elasticity. 1993 1993/06/01;31(3):189-208.

[41] Green AE, Naghdi PM. A re-examination of the basic postulates of thermomechanics. Proceedings of the Royal Society of London Series A: Mathematical and Physical Sciences. 1991;432(1885):171-194.

[42] Othman MIA, Atwa SY, Farouk RM. The effect of diffusion on two-dimensional problem of generalized thermoelasticity with Green–Naghdi theory. International Communications in Heat and Mass Transfer. 2009 2009/10/01/;36(8):857-864.

[43] Green AE, Naghdi PM. On continuum thermodynamics. Archive for Rational Mechanics and Analysis. 1972 1972/01/01;48(5):352-378.

[44] Youssef HM. Theory of Two-Temperature Thermoelasticity without Energy Dissipation. Journal of Thermal Stresses. 2011 2011/01/13;34(2):138-146.

[45] Youssef HM. Theory of generalized thermoelasticity with fractional order strain. Journal of Vibration and Control. 2016;22(18):3840-3857.

[46] Youssef HM. Fractional-order strain of an infinite annular cylinder based on Caputo and Caputo–Fabrizio fractional derivatives under hyperbolic two-temperature generalized thermoelasticity theory. Journal of Umm Al-Qura University for Engineering and Architecture. 2024 2024/07/12.

[47] Youssef HM, El-Bary AA. Vibration of Circular Microplate of Silicon Under Refined Green-Lindsay, Biot, Lord-Sulman, Green-Naghdi Type-1, Green-Naghdi Type-III, and Moore–Gibson–Thompson Theorems of Thermoelasticity. 2025.

[48] Al-Lehaibi EA. Applying Caputo and Caputo–Fabrizio fractional derivatives on a viscothermoelastic circular microplate under Lord–Shulman theorem. AIP Advances. 2025;15(4).

[49] El-Bary AA, Youssef HM, Nasr MAE. Hyperbolic two-temperature generalized thermoelastic infinite medium with cylindrical cavity subjected to the non-Gaussian laser beam. Journal of Umm Al-Qura University for Engineering and Architecture. 2022 2022/12/01;13(1):62-69.

[50] Alghamdi NA. Vibration of circular micro-ceramic (Si3N4) plate resonators in the context of the generalized viscothermoelastic dual-phase-lagging theory. Advances in Mechanical Engineering. 2019;11(11):1687814019889480.

[51] Zhou S, Zhang R, Zhou S, et al. Free vibration analysis of bilayered circular micro-plate including surface effects. Applied Mathematical Modelling. 2019;70:54-66.

[52] Hobiny A, Abbas IA. A GL photo-thermal theory upon new hyperbolic two-temperatures in a semiconductor material. Waves in Random and Complex Media. 2021:1-14.

[53] Youssef HM, El-Bary A. Characterization of the photothermal interaction of a semiconducting solid sphere due to the mechanical damage, ramp-Type heating, and rotation under LS theory. Waves in Random and Complex Media. 2024;34(2):547-572.

[54] Hobiny AD, Abbas IA. The influences of thermal relaxation time and varying thermal conductivity in thermoelastic media. Case Studies in Thermal Engineering. 2024:104263.

[55] Green A, Naghdi P. Thermoelasticity without energy dissipation. Journal of elasticity. 1993;31(3):189-208.

[56] Kumar H, Mukhopadhyay S. Thermoelastic damping analysis in microbeam resonators based on Moore–Gibson–Thompson generalized thermoelasticity theory. ACTA MECHANICA. 2020.

[57] Quintanilla R. Moore–Gibson–Thompson thermoelasticity. Mathematics and Mechanics of Solids. 2019;24(12):4020-4031.

[58] Youssef H. Vibration of gold nanobeam with variable thermal conductivity: state-space approach. Applied Nanoscience. 2013;3(5):397-407.

[59] Youssef HM, El-Bary AA, Elsibai KA. Vibration of gold nano beam in context of two-temperature generalized thermoelasticity subjected to laser pulse. Latin American Journal of Solids and Structures. 2014;11(13):2460-2482.

[60] Al-Lehaibi EA, Youssef HM. Vibration of gold nano-beam with variable young's modulus due to thermal shock. World Journal of Nano Science and Engineering. 2015;5(04):194.

[61] Youssef HM, Alghamdi N. Thermoelastic damping in nanomechanical resonators based on two-temperature generalized thermoelasticity theory. Journal of Thermal Stresses. 2015;38(12):1345-1359.